Video Article

# Evaluation of Stem Cell Therapies in a Bilateral Patellar Tendon Injury Model in Rats

John R. Wagner[1], Takashi Taguchi[1], Jane Y. Cho[2], Chandrashekhar Charavaryamath[3], Dominique J. Griffon[1]

[1]College of Veterinary Medicine, Western University of Health Sciences

[2]Applied Medical

[3]College of Veterinary Medicine, Iowa State University

Correspondence to: Dominique J. Griffon at dgriffon@westernu.edu

URL: https://www.jove.com/video/56810
DOI: doi:10.3791/56810

Keywords: Medicine, Issue 133, Rat model, Tendon injury model, Mesenchymal stem cells, Chitosan, Spheroids, Patellar tendon window defect

Date Published: 3/30/2018

Citation: Wagner, J.R., Taguchi, T., Cho, J.Y., Charavaryamath, C., Griffon, D.J. Evaluation of Stem Cell Therapies in a Bilateral Patellar Tendon Injury Model in Rats. *J. Vis. Exp.* (133), e56810, doi:10.3791/56810 (2018).

## Abstract

Regenerative medicine provides novel alternatives to conditions that challenge traditional treatments. The prevalence and morbidity of tendinopathy across species, combined with the limited healing properties of this tissue, have prompted the search for cellular therapies and propelled the development of experimental models to study their efficacy. Umbilical cord matrix-derived mesenchymal stem cells (UCM-MSC) are appealing candidates because they are abundant, easy to collect, circumvent the ethical concerns and risk of teratoma formation, yet resemble primitive embryonic stem cells more closely than adult tissue-derived MSCs. Significant interest has focused on chitosan as a strategy to enhance the properties of MSCs through spheroid formation. This paper details techniques to isolate UCM-MSCs, prepare spheroids on chitosan film, and analyze the effect of spheroid formation on surface marker expression. Consequently, creation of a bilateral patellar tendon injury model in rats is described for *in vivo* implantation of UCM-MSC spheroids formed on chitosan film. No complication was observed in the study with respect to morbidity, stress rising effects, or tissue infection. The total functional score of the operated rats at 7 days was lower than that of normal rats, but returned to normal within 28 days after surgery. Histological scores of tissue-healing confirmed the presence of a clot in treated defects evaluated at 7 days, absence of foreign body reaction, and progressing healing at 28 days. This bilateral patella tendon defect model controls inter-individual variation via creation of an internal control in each rat, was associated with acceptable morbidity, and allowed detection of differences between untreated tendons and treatments.

## Video Link

The video component of this article can be found at https://www.jove.com/video/56810/

## Introduction

Tendon injury is one of the most common causes of significant pain and muscle atrophy across species[1]. In veterinary medicine, tendon and ligament injuries are of special interest in horses, as 82% of all injuries in race horses involve the musculoskeletal system, and 46% of those affect tendons and ligaments[2,3]. Scar tissue formation affects the biomechanical properties of healed tendons and explains the guarded prognosis for return to athletic use after flexor tendon injuries; re-injury occurs within 2 years in up to 67% of horses treated conservatively[4]. Regenerative medicine provides novel alternatives to a condition that challenges traditional treatments. Autologous stem cell therapy has produced some encouraging results[5,6] but is limited by the morbidity associated with tissue collection, delayed administration due to processing/reprogramming of cells, and the influence of the patient's health status (such as age) on the properties of stem cells[7,8]. These limitations provide a rationale for investigating allogeneic stem cells as an off-the-shelf alternative. Fetal adnexa-derived cells are appealing candidates because they circumvent the ethical concerns and risk of teratoma formation associated with embryonic stem cells. Among fetal adnexa, umbilical cord matrix (UCM), also named Wharton's Jelly, is abundant and easy to collect.

Regardless of cell source, enhancing stemness is essential to establish a cell bank for allogenic regenerative medicine. From a functional standpoint, stemness can be defined as the potential for self-renewal and multi-lineage differentiation[9]. Evidence of stemness relies on proliferation and differentiation assays, along with expression of gene markers *Oct4*, *Sox2,* and *Nanog*[9]. One strategy to enhance stemness relies on the use of biomaterials to serve as void fillers and carriers enhancing proliferation and differentiation of UCM-MSCs. This approach eliminates concerns regarding manipulation of transcriptional factors to reprogram mature cells into induced pluripotent cells. Among biomaterials considered as potential carriers for stem cells, chitosan is appealing for its biocompatibility and degradability[10]. This natural aminopolysaccharide is formed by alkaline deacetylation of chitin, the second most abundant natural polysaccharide, primarily obtained as a subproduct of shellfish[10]. We have previously investigated interactions between MSCs and chitosan scaffolds, and observed the formation of spheroids[11,12,13,14,15,16]. We also reported on the superiority of chondrogenesis on chitosan matrices[12,13,14,15,16,17,18]. More recently, two independent studies described spheroids formation by adipose tissue and placenta tissue derived MSCs cultured on a chitosan film[19,20]. This formation of spheroids not only enhanced stemness, but also improved the retention of stem cells after *in vivo* implantation[20].

 

The prevalence and morbidity of tendinopathy across species have prompted the development of experimental models to study the pathophysiology of tendinopathies and test new therapies such as stem cell injections. In horses, collagenase-induced tendonitis is a common model to demonstrate efficacy using MSCs in tendon repair[21]. The relevance of this approach is limited, as injections cause acute inflammatory changes, whereas clinical tendinopathies usually result from chronic overstrain[22,23]. In addition, chemical induction of tendon disease induces a healing response and does not replicate the impaired healing process present in clinical cases[22,23]. Excision of a segment of the superficial digital flexor tendon has been described as a surgical model of tendonitis in horses[24]. More recently, a minimally invasive approach was used to restrict the traumatic damage to the central core of the superficial digital flexor tendon[25]. Surgical models do not simulate the fatigue mechanism that may lead to natural tendon disease, and tend to lack reproducibility in the extent of damage created[25]. Regardless of the model, the morbidity and cost associated with equine models of tendon diseases are additional limitations, which justify an interest in rodent models as a first step for *in vivo* evaluation of novel therapies.

One of the main advantages of experimental models in rodents consists of the cost and ability to control inter-individual variability. Rodents can be standardized with respect to various physiological factors due to their rapid growth rates and relatively short life spans, limiting sources of variation and therefore reducing the number of animals required to detect differences. Strategies to induce tendon diseases in rodents have relied on chemical induction, but also on surgical creation of partial tendon defects[21]. Surgical models may simulate natural tendinopathies better than chemical models, but can lead to higher morbidity and catastrophic failure of the damaged tendon. In that respect, rats seem better candidates than mice for these models, as their size allows creation of larger defects, thereby facilitating evaluation of tissue healing. Sprague-Dawley rats have been used in experimental studies of tendinopathies in four major tendon groups: rotator cuff, flexor, Achilles, and patellar tendons[26]. Among these, models involving the patellar tendon are especially appealing because of the larger size of this tendon and the ease of accessing it[27]. The patellar tendon attaches the quadriceps muscle to the tibial tuberosity. Within this extensor mechanism, the patella is a sesamoid bone that directs the action of the quadriceps and delineates the proximal extent of the patellar tendon. The presence of bony anchors at the proximal and distal extents of the patellar tendon facilitates biomechanical tests. Models involving the patellar tendon typically rely on unilateral surgical defects, with a contralateral intact tendon serving as a control[28,29]. The most common patellar tendon defect model involves excising the central portion (1 mm in width) of the patellar tendon from the distal apex of the patella to the insertion of the tibial tuberosity, while the contralateral patellar tendon is left intact. Measures of outcomes have included histology, non-destructive biomechanical testing or biomechanical testing to failure, ultrasound imaging, *ex vivo* fluorescence imaging, gross observation, and functional tests[28,30,31]. Unilateral models do not allow comparison of a proposed treatment with conservative management of a similar injury within the same animal. Similarly, comparison between several treatments requires separate animals. A bilateral model would eliminate inter-individual variations and reduce the number of animals required for a study[32]. However, bilateral injuries may increase morbidity, and bilateral lameness could impede treatment evaluation. A few studies briefly report the use of bilateral patellar tendon defects in rats but focus on the effects of treatments rather than peri-operative management and morbidity of the model[33,34].

This study's long-term goal is to develop a strategy to improve stemness and *in vivo* survival of UCM-MSCs destined to allogenic transplantation. To achieve this goal, we have recently reported improved stemness of UCM-MSCs by formation of spheroids on chitosan film and incubation under hypoxic environment[35]. These *in vitro* properties were associated with improved biomechanical properties of patellar tendon defects treated with conditioned UCM-MSCs. Based on these results, the rat bilateral patellar tendon defect model seems suitable to test candidate treatments for tendon injuries[36]. The purpose of the study reported here is to provide detailed protocols for isolation and characterization of UCM-MSCs, preparation of a biologic delivery system for stem cells, creation and treatment of bilateral patella tendon defects, and post-operative recovery and evaluation of tissue healing within the defects.

## Protocol

All methods described here have been approved by the Institutional Animal Care and Use Committee (IACUC) of Western University of Health Sciences.

# 1. Isolation and Expansion of MSCs from Equine Umbilical Cord Matrix

1. Obtain the placenta from an adult mare (pregnant) after observed foaling and aseptically isolate the umbilical cord from the placenta. Keep the umbilical cord in phosphate buffered saline (PBS) with 1% penicillin-streptomycin (P/S) at 4 °C during transfer until processing.
2. Wash the umbilical cord twice with room temperature PBS with 1% P/S in a 50 mL tube. Section the umbilical cord into 2-inch-long fragments on 150 mm plate and wash in room temperature PBS with 1% P/S in a 50 mL tube two or three times, until most of the blood is rinsed out.
3. Cut the umbilical cord longitudinally to expose vessels. Remove vessels, including 2 arteries, a vein, and an allantoic stalk from the cord using forceps and scissors. Collect umbilical cord matrix (Wharton's Jelly), which is the jelly-like matrix surrounding vessels, onto a 150 mm plate by scraping with a scalpel, and mince the jelly into fine pieces.
4. Place Wharton's Jelly from 2–3 umbilical cord fragments (approximately 12–15 g) in a 50-mL tube with 15 mL of 0.1% (w/v) collagenase type IA solution in PBS. Incubate at 37 °C with gentle shaking for 3-4 h until dissolved.
5. Centrifuge digested tissue at 300 x g for 15 min and aspirate supernatant. Resuspend digested tissue in 15 mL of room temperature PBS with 1% P/S, mix by pipetting, centrifuge at 150 x g for 5 min, and aspirate supernatant (wash). Repeat washing twice more.
6. Resuspend washed cells in 15 mL of room temperature PBS with 1% P/S, mix by pipetting, strain by with 100 µm cell strainer, centrifuge at 150 x g for 5 min, and aspirate supernatant.
7. Prepare culture medium (CM) by mixing low glucose Dulbecco's Modified Eagle's Medium (LG-DMEM) with fetal bovine serum (FBS) and 1% P/S. Sterilize the medium by filtration.
8. Resuspend strained cells in 10 mL of CM pre-warmed to 37 °C, mix by pipetting, transfer into a 25 $cm^2$ tissue culture flask, and incubate in 5% $CO_2$ at 90% humidity and 37.0 °C. Change CM every 3 days until the culture reaches 70–80% confluence, when the culture will be passaged.
9. To passage the culture, aspirate CM from flask, wash with 5 mL of room temperature PBS twice, and detach with 3 mL of 0.25% trypsin/ethylenediaminetetraacetic acid (EDTA) at 37 °C for 5 min.

10. Neutralize trypsin/EDTA with 6 mL of CM pre-warmed to 37.0 °C, mix by pipetting, transfer into a 15 mL tube, centrifuge at 150 x g for 5 min, and aspirate supernatant. Resuspend detached cells in 1 mL of CM, mix by pipetting. Count the viable cells using trypan blue and hemocytometer. Re-seed into a 25 $cm^2$ tissue culture flask at 5,000 cells/$cm^2$, and incubate in 5% $CO_2$ at 90% humidity and 37.0 °C.

## 2. Preparation of Spheroids with UCM-MSCs Cultured on Chitosan Films

1. To prepare 100 mL of 1% (w/v) chitosan solution, add 1 g of chitosan in 99 mL of distilled water ($dH_2O$), and mix well with a magnetic stirrer.
2. Add 670 µL of glacial acetic acid and continue mixing until chitosan dissolves and becomes viscous. This usually takes 3–4 h.
3. Add 500 µL of chitosan solution into each well of the 12-well tissue culture plate, and swirl the plate to distribute chitosan solution evenly and cover all of the bottom surface.
4. Dry the chitosan solution coated plate under laminar flow cabinet without a cover overnight for 24 h. Once dried, thin film will be formed and adhered to plate.
5. Neutralize chitosan film by adding 1 mL of 0.5 N sodium hydroxide (NaOH) solution into each well and incubate for 2 h at room temperature. Aspirate NaOH from each well and wash each well with 1 mL of $dH_2O$ three times. Wash each well with 1 mL of 70% ethanol (EtOH) once.
6. To sterilize chitosan film, add 1 mL of 70% EtOH into each well and incubate overnight in laminar flow cabinet. Aspirate remaining EtOH from each well in the following day. Wash each well with 1 mL of sterile PBS three times. Sterilize chitosan film with ultraviolet light under laminar flow cabinet overnight without a cover.
7. To form spheroids of UCM-MSCs, seed expanded and passaged cells into each well at 5,000 cells/$cm^2$, and incubate in 5% $CO_2$ at 90% humidity and 37.0 °C.
   NOTE: Cells can be incubated under hypoxia or normoxia, depending on the investigator's interest.

## 3. Expression of Surface Markers Analyzed via Flow Cytometry

1. **Preparation of a single cell suspension**
   1. Standard plate
      1. Remove medium from each well and wash twice with room temperature PBS.
      2. Detach cells with 500 µL of a cell dissociation reagent into each well of a 12-well plate for 5–10 min at room temperature.
      3. After incubation, add 1 ml of staining buffer (PBS containing 0.5% BSA) into each well and mix by pipetting to detach cells.
      4. Transfer cell suspension into 15 mL conical tube and centrifuge at 150 x g for 5 min.
   2. Chitosan plate
      1. Collect all spheroids by aspirating medium using a pipette with a 1,000 µL tip. Transfer collected medium into a 15-mL conical tube. After collecting medium, wash well by adding 1 mL of PBS, and transfer washed PBS into the same 15 mL conical tube.
      2. Centrifuge spheroids at 150 x g for 5 min and remove supernatant.
      3. Add 500 µL of the cell dissociation reagent (*e.g.*, accutase) and incubate for 5–10 min at room temperature. Mix by pipetting using a 1 mL tip until spheroids dissociate and are no longer visible.
      4. Add 1 mL of staining buffer into the single cell suspension and centrifuge at 150 x g for 5 min.

2. **Washing cells**
   1. Remove the supernatant from the conical tube and re-suspend the cells in 3 mL of cold staining buffer. Keep cells on ice throughout experiment from this step.
   2. Centrifuge at 300 x g for 5 min (washing).
   3. Wash twice.

3. **Staining cells**
   1. Centrifuge at 300 x g for 5 min and remove supernatant.
   2. Count viable cells using a trypan blue and hemocytometer. Re-suspend 1 x $10^6$ cells in 50 µL blocking buffer (PBS containing 10% horse serum) and incubate for 30 min on ice.
   3. Add 10 µL fluorescein isothiocyanate (FITC) conjugated antibodies (CD44, CD90, CD105, CD34, major histocompatibility complex (MHC) class II, or isotype control for each antibody) and 40 µL of staining buffer, then incubate protected from light for 1 h on ice.
   4. Add 3 mL of cold staining buffer and mix, centrifuge at 300 x g for 5 min, and aspirate supernatant (washing).
   5. Repeat washing twice.
   6. Re-suspend the cell pellet in 0.5 mL of staining buffer
   7. Add 5 µL of 7-AAD (viability dye) and incubate for 30 min on ice
   8. Analyze stained cell samples by flow cytometer. Exclude debris by their smaller SSC and FSC, and identify viable cells with lower uptake of 7-AAD. Plot FL1 and FL2 on the y- and x- axes, respectively. Use isotype control to create a gate above the diagonal line. Measure the percentage of positively stained cells in the area. Count at least 20,000 events/sample (**Supplementary Figure 1**).
   9. Measure the percentage of cells stained with antibodies by gating viable cells and auto-fluorescence, and subtract percentage of cells stained with isotype control.

## 4. Bilateral Patellar Tendon Defect Model in the Rat

1. Select Sprague-Dawley rats (adult male, 4–5 months old, body weight 350–375 g). Note the relatively large size of the rats used for this model.
2. Anesthetize and apply artificial eye lubricant the rat with 8% sevoflurane in 2 L/min 100% oxygen delivered via mask, until disappearance of pinch-toe reflex in the induction chamber.
3. Administer an intramuscular injection of Meloxicam (1 mg/kg) as preemptive analgesia.

4. Place the rat between two 0.5 L water bottles filled with warm water and covered with a cloth to maintain body temperature and position, while preventing skin injury. Tape each extremity to the table. To reduce risk of hypothermia, cover the body with bubble wrap (**Figure 1**).
5. Maintain anesthesia with continuous flow of 5% sevoflurane in 1 L 100% oxygen mixture via nose cone, with the animal on dorsal recumbency on water heating pad.
6. To avoid skin trauma, do not clip the surgical sites. Instead, apply hair remover cream over both stifles. Use a tongue depressor to remove the cream and hair.
7. Scrub the surgical site with chlorhexidine digluconate scrub, and rinse with 70% ethanol 3 times.
8. Incise the skin with a sterile #15 scalpel blade in a proximal to distal direction, on the craniomedial aspect of the stifle. Start the incision about 1 cm proximal to the level of the patella, and extend it approximately 5 mm distal to the tibial tubercle.
9. Reflect the skin to expose the patellar tendon by freeing the underlying subcutaneous tissue with a #15 scalpel blade.
10. **Using the #15 scalpel blade, excise the central third of each patellar tendon (1 mm) from the distal aspect of the patella to the tibial tuberosity.**
    1. Align a 0.99 mm-diameter Kirschner wire against the tendon as a template to standardize the size of the defect in each limb (**Figure 2**).
    2. Make 2 full-thickness incisions on each side of the Kirschner wire with a #15 scalpel blade to isolate the central portion of the tendon (**Figure 3**). Resect the central section proximally and distally with fine Iris scissors (**Figure 4**).
    3. Before closing the fascia of the stifle, insert the clot (mixed cell suspension and ACP) for the appropriate treatment groups as described in 5.5. Close the fascia with a cruciate pattern and skin with an intradermal pattern using 5-0 polyglactin 910 sutures (**Figure 5**).
11. Repeat the procedure on the contralateral stifle.
    NOTE: One defect is randomly assigned to a treatment (stem cells conditioned on chitosan or cultured on standard plates). The contralateral defect is left empty, to serve as internal control.
12. After surgery, administer 4 tablets of enrofloxacin (2 mg/tablet, orally, once daily) and a tablet of meloxicam (2 mg/tablet, orally, once daily) for 7 days. These doses were recommended by a laboratory animal veterinarian and approved in the IACUC protocol.

## 5. Delivery of MSCs within the Patellar Tendon Defect

1. Anesthetize a healthy rat which is not used for patellar tendon defect creation with 8% sevoflurane in 2 L/min 100 % oxygen delivered via mask, until disappearance of pinch-toe reflex in the induction chamber.
2. Collect 5 mL blood by cardiac puncture from the anesthetized Sprague-Dawley rat (adult male, 4–5 months old, body weight 350–375 g), in a 5 mL syringe with a 20 G needle containing 1 mL of acid-citrate-dextrose (5:1 v/v).
3. Euthanize the rat after cardiac puncture and blood collection, by intracardial injection of pentobarbital (100 mg/kg), while under the same anesthesia.
4. Centrifuge the sample at 350 x g for 15 min at room temperature. Transfer supernatant and store aliquots (120 µL each) at -20 °C until use.
5. Immediately before *in vivo* implantation, thaw the above aliquot and mix 20 µL with 0.5 x $10^6$ MSCs (from either 1.9 or 3.1.2.1) detached from standard plates using trypsin/EDTA, or collect from chitosan plates by flushing (with PBS/medium).
6. Add 6 µL of 10% calcium chloride ($CaCl_2$) to the remaining 100 µL of thawed plasma in a well of 96-well plate to activate the plasma and induce formation of a clot (activated conditioned plasma: ACP).
7. Mix cell suspension (20 µL) and ACP (100 µL) to form a clot (**Figure 6**). Place the clot within the patellar tendon defect created before closing the fascia of the stifle (see step 4.10.3).

## 6. Functional Outcome

1. Monitor rats twice a day for signs of pain, based on the rat grimace scale (RGS)[37,38] and swelling over the implantation sites.
   NOTE: A scoring system (0–6) was developed to evaluate ambulatory function based on 3 activities, including timed hind limb standing with forelimbs supported (0-3), timed unassisted hind limb standing (0–2), and the ability to climb a 17 cm plastic cage wall (0–1) (**Table 1**).
2. Evaluate rats for the two hind limb standing activities in the morning and in the evening of each time point to calculate an average score.
3. Evaluate rats for the ability to successfully climb a 17 cm plastic cage wall with both hind limbs reaching the top.

## 7. Gross Appearance and Histopathology of the Patellar Tendon

1. Euthanize rats at 7 days (to evaluate inflammation) or 28 days (to evaluate tissue healing) post treatment by intracardial injection of pentobarbital (100 mg/kg) under anesthesia with 8 % sevoflurane and 2 L 100% oxygen delivered via mask.
2. Harvest patella-tendon-tibia tuberosity units by scalpel and scissors after euthanasia. Remove soft tissues and ligaments around the stifle, except for the patellar tendon.
3. Examine each specimen for gross appearance and thickening of the tendon (**Figure 7**).
4. Orient the specimen by placing a surgeon's knot of 5.0 Polydioxanone on the proximal and lateral aspect of the tendon. Fix each specimen in 10% neutral buffered formalin solution and obtain transverse sections (5 µm) from the mid-portion of each tendon.
5. Stain the sections using hematoxylin and eosin, and Masson's Trichrome staining following standard protocols.
6. Examine section to detect the presence of hematoma within the defect, as well as pathological changes such as inflammation.
7. Evaluate the histological score of sections using the previously published scoring system, based on collagen grade, degree of angiogenesis, and cartilage formation (**Table 2**)[39].

## Representative Results

In the current study, results are presented as mean ± SD (standard deviation). Cells were isolated from the umbilical cords of 6 mares, and percentage of isolated cell lines expressing each cell surface marker under standard or chitosan conditioning were compared with a Friedman test, as a non-parametric analysis of variance with repeated measures. For tendon defect model creation, 8 rats were used for 7 days post-surgery assessment and 12 rats were used for 28 days assessment. Results of functional outcomes are presented as mean ± SEM (standard error of the mean) and compared using the t-test. UCM was selected as a cellular source due to its abundance, ease of collection, and superior proliferation relative to other fetal adnexa sources[40]. Cells isolated from UCM cultured on standard plates maintained a fibroblast-like shape throughout the expansion. Cells formed spheroids when cultured on chitosan plate (**Figure 8**).

The majority of cells cultured under standard conditions expressed CD44 (98.6 ± 1.62%), CD90 (88.7 ± 3.04%), and CD105 (77.9 ± 6.84%), while expression of CD34 (0.07 ± 0.17%) and MHC II (1.33 ± 1.12%) were very low. Under conditioned culture, the expression levels of CD44 (97.0 ± 2.12%) and CD34 (1.13 ± 1.58%) did not differ from standard cultures, while expression levels of CD90 (33.3 ± 37.1%) and CD105 (54.0 ± 19.0%) decreased and MHC II (2.84 ± 0.98%) increased[35].

Following isolation and characterization of UCM-MSCs *in vitro*, the biological behavior of conditioned cells was compared to that of cells cultured under standard conditions in a bilateral patellar tendon defect model in rats. Untreated defects in each rat served as internal controls. Post-operative swelling was minimal in all rats and resolved within 48 h. According to the RGS, none of the rats displayed signs of pain or distress such as orbital tightening, nose/cheek flattening, or ear/whisker changes. All rats consumed a normal range of 3–4 pellets or 15–20 grams of feed daily throughout the study. The total functional score, including assisted and unassisted hind limb standing as well as climbing scores was higher in normal rats compared to that of operated rats at 7 days ($n = 8$, $p < 0.0001$, **Table 3**). However, the total functional score returned to normal within 28 days after surgery ($n = 12$, $p = 0.78$). Therefore, rat bilateral patellar tendon defect models have been shown to be effective for limiting inter-individual variation and reducing the necessary number of animals without causing significant morbidity (**Video 1**–**5**).

About 37% of tendons collected at 28 days appeared markedly thickened (**Figure 7**). This thickening was equally distributed between empty and treated defects. Total histological scores increased with time in untreated defects ($n = 20$, $p = 0.0034$). When each component of the healing score was evaluated independently, the only parameter changing with time consisted of cartilage formation, which increased between 7 and 28 days ($n = 20$, $p < 0.0001$). Angiogenesis tended to increase with time ($p = 0.3$), but collagen formation did not differ ($p = 0.69$). Upon histological examination, inflammation was observed in all of the tendons' tissue sections examined at 7 days after surgery, regardless of the presence of treatment. A hematoma was present in all treated defects. Histological angiogenesis scores (**Table 2, Figure 9**) ranged from 0 to 1, suggesting moderate arteriole and capillary infiltration, while collagen grade scores (**Table 2, Figure 10**) ranged from 2 to 3 overall, suggesting moderate to extensive collagen formation. Cartilage formation scores (**Table 2, Figure 11**) ranged from 0 to 2 suggesting no cartilage formation, to moderate cartilage formation of 25% to 50% of the tendon section area. All histological figures are oriented with the left side as the anterior aspect, and the top as the medial aspect of the transverse section of the mid-portion of the tendon.

**Figure 1: Positioning of rats and preparation for aseptic surgery.** Each rat was placed between two 0.5 L water bottles filled with warm water and covered with a cloth to maintain body temperature and position, while preventing skin injury. The extremities of each rat were taped to the table and its body was covered with bubble wrap. Please click here to view a larger version of this figure.

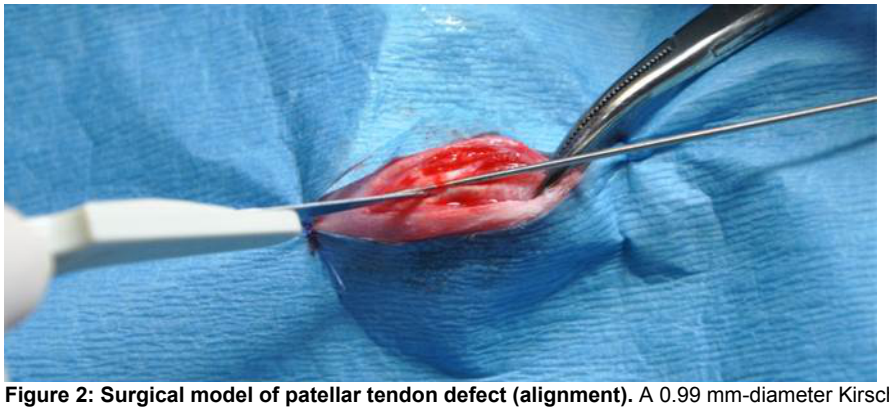

**Figure 2: Surgical model of patellar tendon defect (alignment).** A 0.99 mm-diameter Kirschner wire is aligned against the tendon as a template to standardize the size of the defect in each limb.

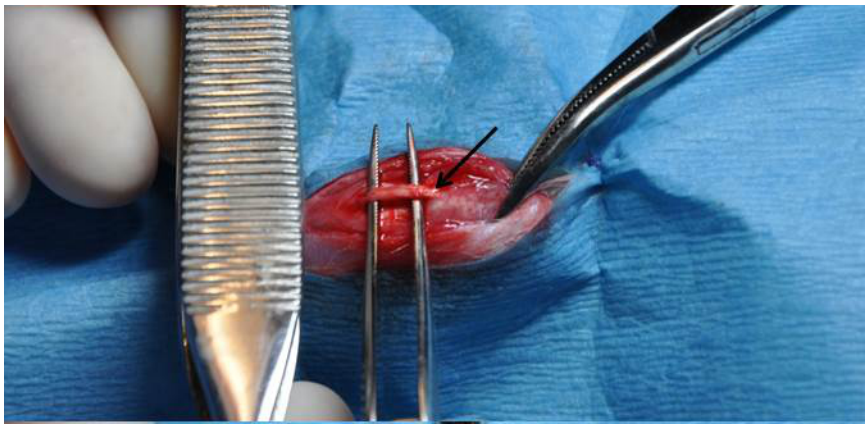

**Figure 3: Surgical model of patellar tendon defect (incisions).** Two full-thickness incisions are made on each side of the Kirschner wire to isolate a central portion of the tendon.

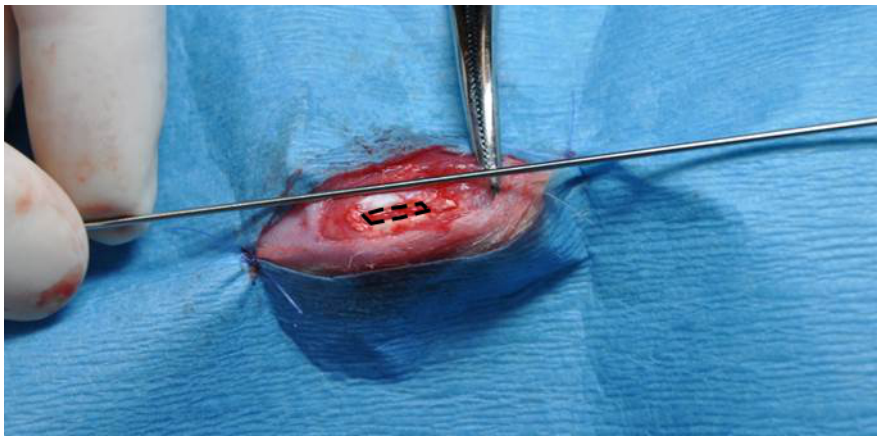

**Figure 4: Surgical model of patellar tendon defect (resection).** The central section is resected proximally and distally, creating a defect matching the size of the Kirschner wire. Resected area is shown within dotted line box.

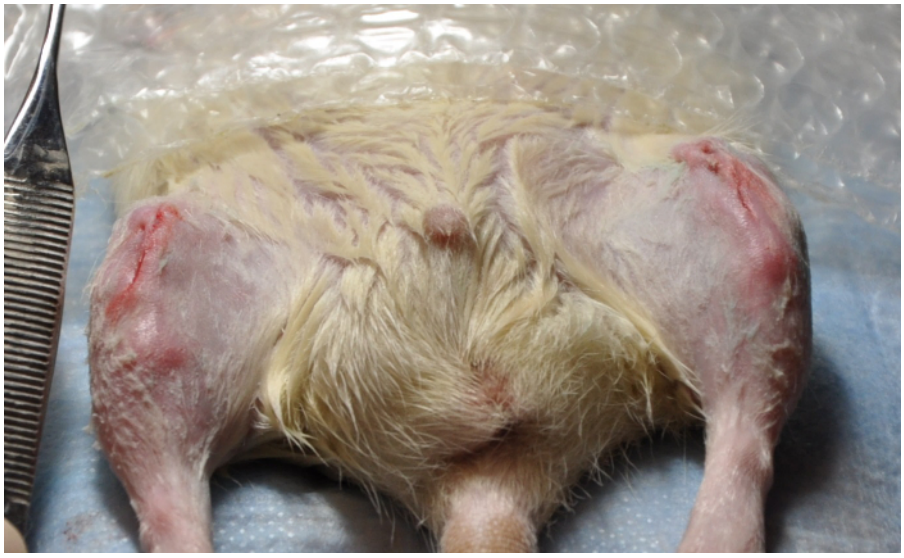

**Figure 5: Post-operative appearance of operated stifles.** Fascia was closed with a cruciate pattern and skin was closed with an intradermal pattern. Please click here to view a larger version of this figure.

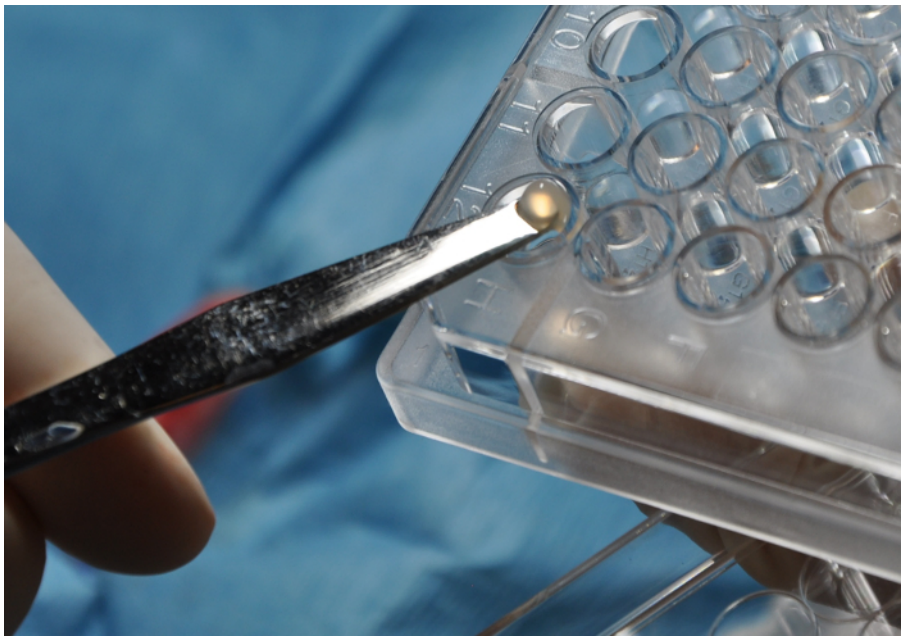

**Figure 6: Preparation of activated conditioned plasma for delivery of UCM-MSCs.** Stem cells were suspended in conditioned plasma prior to activation. The resulting clot was inserted into patellar tendon defects. Please click here to view a larger version of this figure.

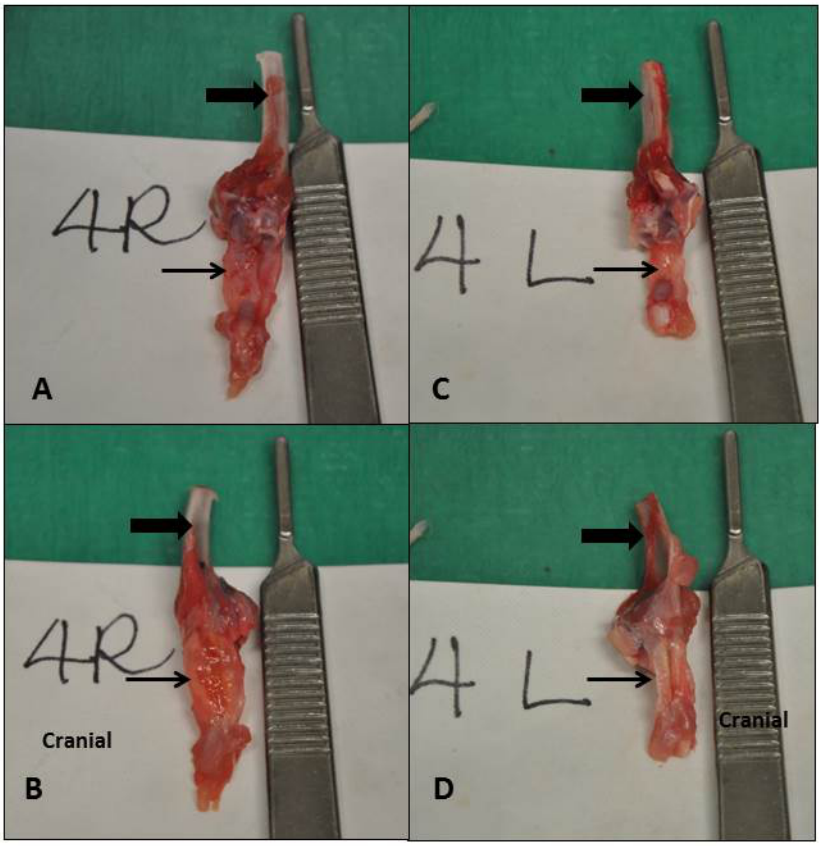


**Figure 7:** Gross appearance of normal (**C**, **D**) and thickened (**A**, **B**) tendons. (**A**, **C**) Posterior views; (**B**, **D**) Lateral views; Block arrows identify the tibia and thin arrows identify the tendons.

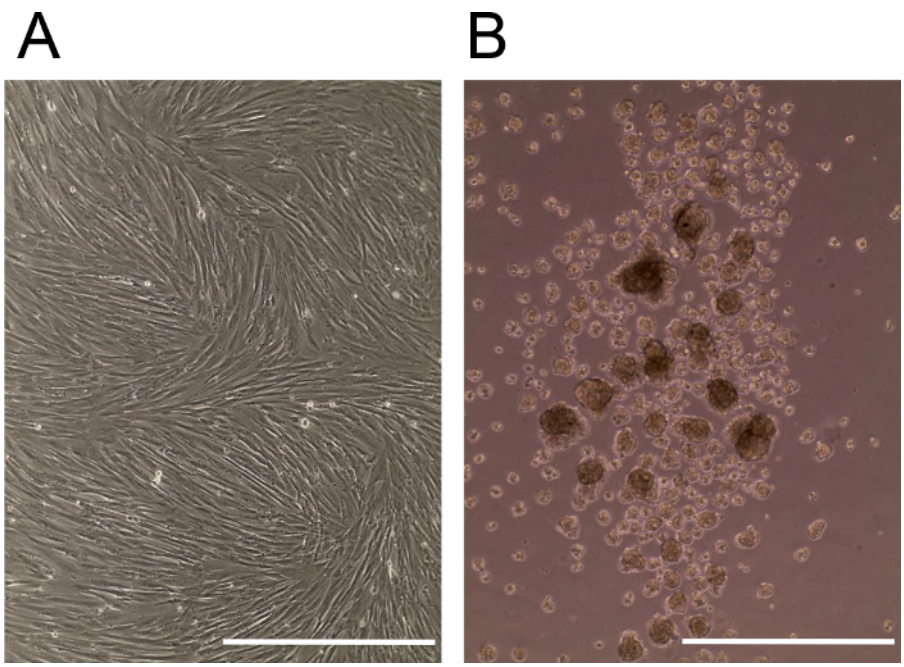


**Figure 8: Morphology of cells cultured on tissue culture plate under 19% oxygen level (standard group: A) and chitosan film under 5% oxygen level (conditioned group: B).** Isolated cells were spindle shaped on standard group (**A**) and formed spheroids on conditioned group (**B**). Scale bar = 400 µm Please click here to view a larger version of this figure.

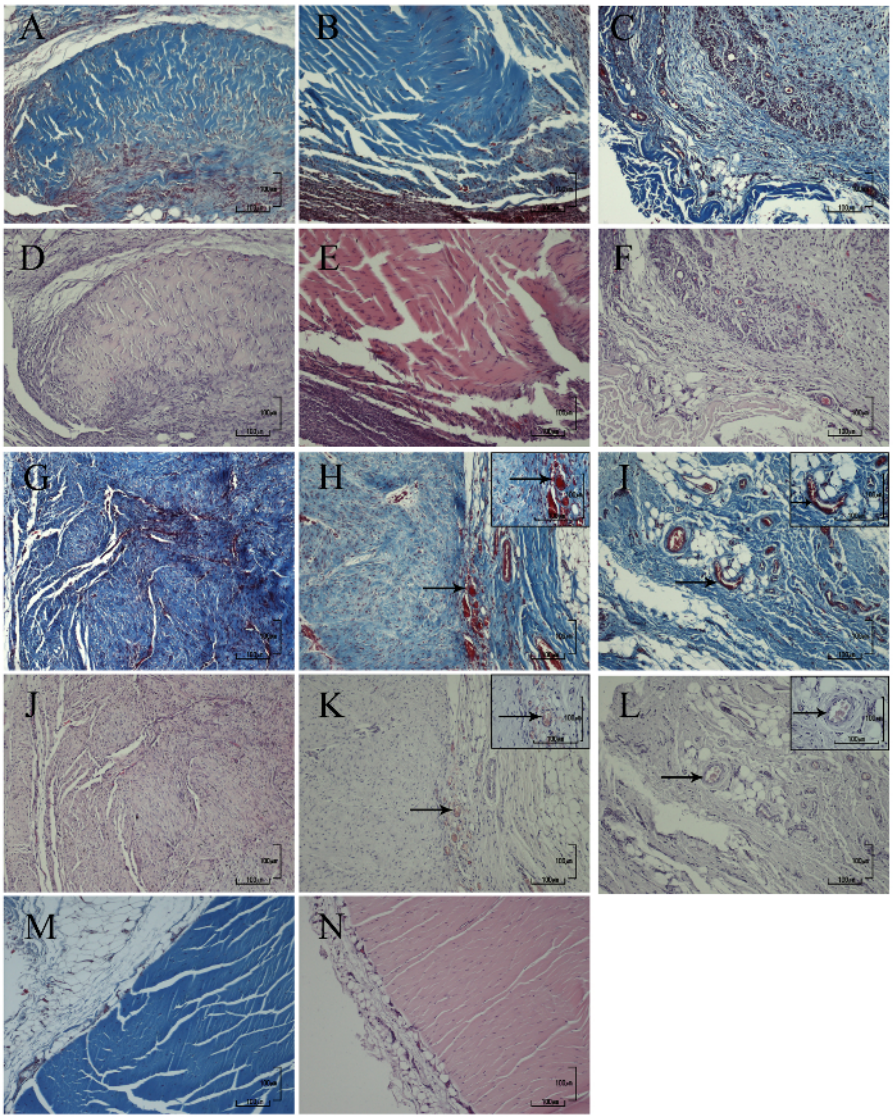


**Figure 9: Representative light micrographs used for angiogenesis grading.** Following 7 days of healing, tendons with no treatment received a grade of 0 (**A**, **D**), whereas those with either conditioned cells (**C**, **F**) or standard cells (**B**, **E**) received a grade of 0.5 and 0, respectively. At 28 days, untreated tendons (**G**, **J**) received a grade of 0, whereas those with conditioned cells (**I**,**L**) or standard cells (**H**,**K**) received scores of 1.0 and 0.5, respectively. The arrows identify blood vessels present in the tendon sample. The arrows pointing to the blood vessels in 100X magnification correspond to the same arrows pointing to the blood vessels in the 400x magnification. Normal tendon tissue (**M**, **N**). Masson's trichrome stain (**A, B, C, G, H, I, M**); hematoxylin and eosin stain (**D, E, F, J, K, L, N**); Scale bar = 100 μm (**A-N**). Please click here to view a larger version of this figure.

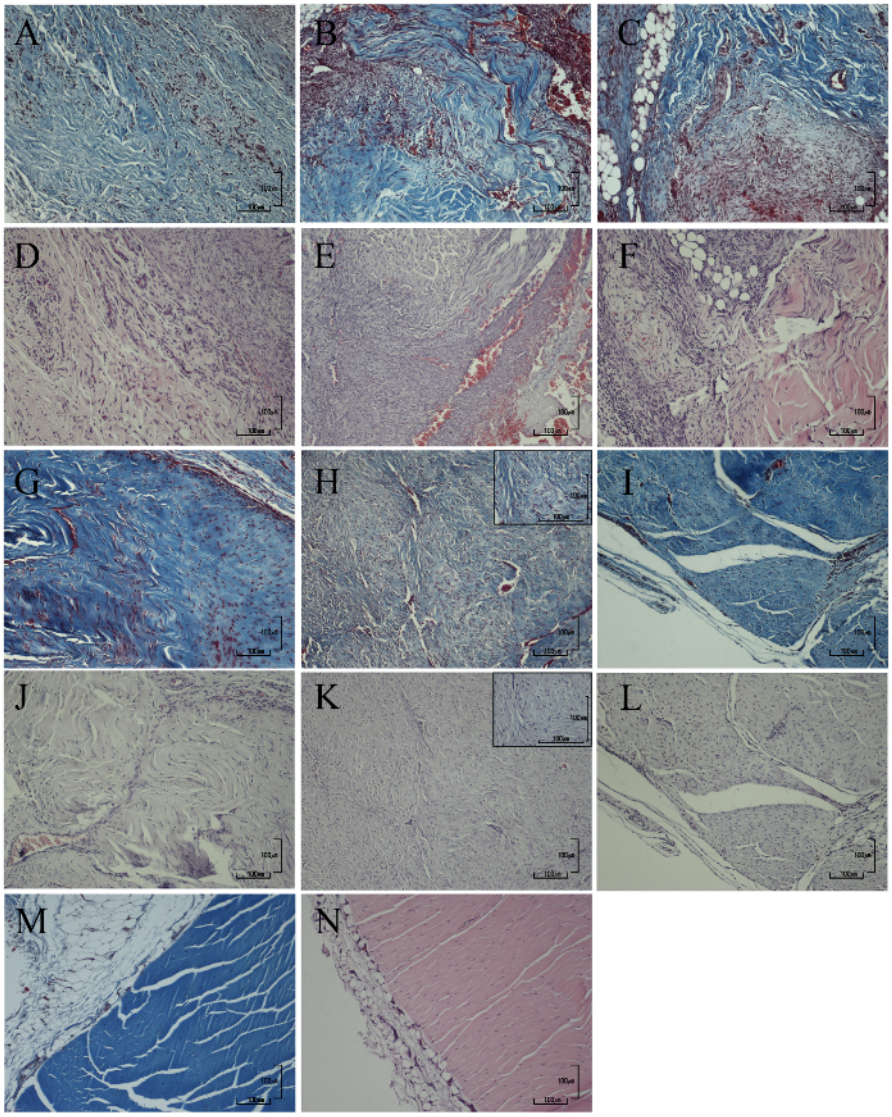


**Figure 10: Representative light micrographs used for collagen grading.** Following 7 days of healing, tendons with no treatment received a grade of 2.5 (**A, D**) whereas those with treatment (**B, C, E, F**) received a grade of 3.0. At 28 days, untreated tendons (**G, J**) received a grade of 3.0, whereas those with conditioned cells (**I, L**) or standard cells (**H, K**) received scores of 1.0 and 3.0, respectively. The disorganization of the tendon fibers can be appreciated in 400X insets (**H, K**). Normal tendon tissue (**M, N**). Masson's trichrome stain (**A, B, C, G, H, I, M**); hematoxylin and eosin stain (**D, E, F, J, K, L, N**); Scale bar = 100 µm (**A-N**). Please click here to view a larger version of this figure.

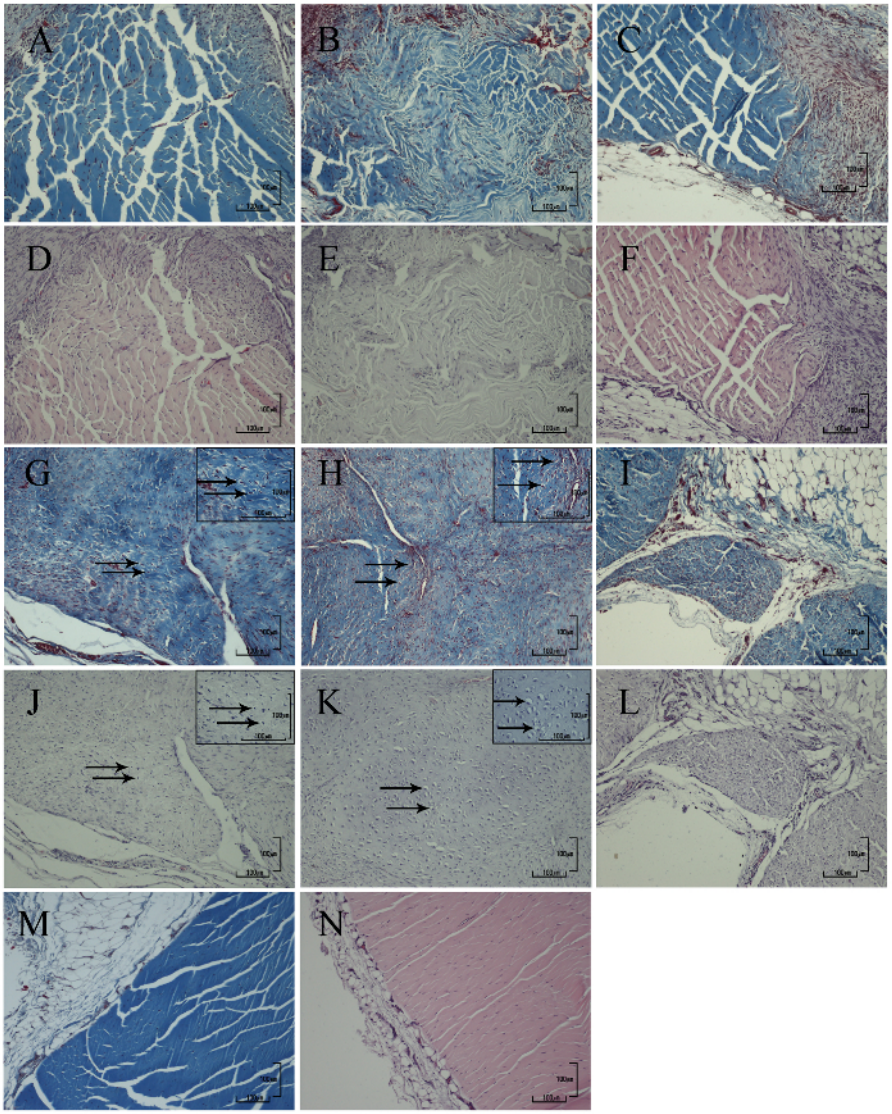


**Figure 11: Representative light micrographs used for cartilage grading.** Following 7 days of healing, tendons with no treatment (**A, D**), those with either conditioned cells (**C, F**) or standard cells (**B, E**), all received a grade of 0. At 28 days, untreated tendons (**G, J**) received a grade of 1.0, whereas those with conditioned cells (**I, L**) or standard cells (**H, K**) received scores of 0 and 2.0, respectively. The arrows are pointing at chondrocytes present in the tendon sample. The arrows pointing to the chondrocytes in 100X magnification correspond to the same arrows pointing to the chondrocytes in the 400X magnification. Normal tendon tissue (**M, N**). Masson's trichrome stain (**A, B, C, G, H, I, M**); hematoxylin and eosin stain (**D, E, F, J, K, L, N**); Scale bar = 100 µm (**A-N**). Please click here to view a larger version of this figure.

**Video 1: Evaluation of ambulatory function in rats**. Timed unassisted hind limb standing (1–5 s: score 1) was observed 4 h post-operatively. Please click here to view this video. (Right-click to download.)

**Video 2: Evaluation of ambulatory function in rats.** Timed hind limb standing with forelimbs assisted (0–5 s: score 0) was noted 4 h post operatively. Please click here to view this video. (Right-click to download.)

**Video 3: Evaluation of ambulatory function in rats**. Timed unassisted hind limb standing (1–5 s: score 1), timed hind limb standing with forelimbs assisted (5–10 s: score 1) was noted 14 days post operatively. Please click here to view this video. (Right-click to download.)

**Video 4: Evaluation of ambulatory function in rats.** Timed hind limb standing with forelimbs assisted (10–15 s: score 2), without the ability to climb a 17 cm plastic cage wall (No climbing: score 0) was noted 27 days post operatively. Please click here to view this video. (Right-click to download.)

**Video 5: Evaluation of ambulatory function in rats.** Timed hind limb standing with forelimbs assisted (5–10 s: score 1), with the ability to climb a 17 cm plastic cage wall (Yes: score 1) was noted 14 days post operatively. Please click here to view this video. (Right-click to download.)

| Functional Test | 0 | 1 | 2 | 3 | Score |
|---|---|---|---|---|---|
| Hind limb stand assisted | 0–5 s | >5–10 s | >10–15 s | >15 s | |
| Hind limb stand unassisted | 0–1 s | >1–5 s | >5 s | | |
| Climbing ability | No | Yes | | | |
| | | | | **Total** | |

**Table 1: Scoring system to evaluate ambulatory function in rats**. A scoring system (0–6) was developed to evaluate ambulatory function based on 3 activities including timed hind limb standing with forelimbs supported (0–3), timed unassisted hind limb standing (0–2), and the ability to climb a 17 cm plastic cage wall (0–1).

| **Collagen grade** | |
|---|---|
| 0 | Normal collagen oriented tangentially |
| 1 | Mild changes with collagen fibers less than 25% disorganized |
| 2 | Moderate changes with collagen fibers between 25% and 50% disorganized |
| 3 | Marked changes with collagen more than 50% disorganized |
| **Degree of angiogenesis** | |
| 0 | Moderate infiltration of tissue with arterioles |
| 1 | Presence of capillaries |
| 2 | No vasculature infiltration |
| **Cartilage formation** | |
| 0 | No cartilage formation |
| 1 | Isolated hyaline cartilage nodules |
| 2 | Moderate cartilage formation of 25% to 50% |
| 3 | Extensive cartilage formation, more than 50% of the field involved |

**Table 2: Histology scoring grades.** Histological score of sections were graded based on collagen grade, degree of angiogenesis, and cartilage formation (adapted from Rosenbaum *et al.*[39])

| Group | Mean ± SEM |
|---|---|
| Normal (n = 3) | 6.00 ± 0.48 |
| 7 days after surgery (n = 8) | 2.25 ± 0.30 |
| 28 days after surgery (n = 12) | 5.83 ± 0.24 |

**Table 3: Functional scores of normal rats and untreated rats.** Functional scores of normal rats and untreated rats 7 and 28 days postoperatively were graded. n = number of rats.

**Supplementary Figure 1: Gating strategy and example of surface marker expression:** Debris was excluded based on small FSC and SSC (**A**). Live cells were selected based on negative staining with 7-AAD detected by FL3 (**B**). Isotype matched control (**C**) was used as negative control to create a gate of CD44-FITC positive cells (**D**).

## Discussion

Equine cells were selected for this project because we eventually intend to test candidate approaches in the management of natural tendinopathies in horses. Indeed, tendon injuries in horses are appealing as natural models of tendinopathy in man because of the biological similarity between the equine superficial digital flexor and Achilles tendon in humans[41]. The cell surface markers CD44, CD90, CD105, CD34, and MHC II were selected for immunophenotyping of cells, in accordance with the criteria recommended by the International Society for Cellular Therapy[42]. In a recent study, eqUCM-MSCs were positive for CD44 and negative for CD34 and MHC II, regardless of culture conditions. Cells cultured under standard conditions were also positive for CD90 and CD105, thereby meeting the criteria for MSCs in terms of expression of surface markers. Additionally, this study is the first report on the formation of spheroids when eqUCM-MSCs are cultured on chitosan film, confirming previous reports on human MSCs[19,20]. 3D cell culture techniques have been extensively explored for decades aiming to create an environment resembling the physiological niche. Indeed, this study showed improved stemness gene expression levels of *Oct4*, *Sox2*, and *Nanog*, and improved differentiation potential, which is consistent with other reports[19,20]. Others reported improved immunomodulatory properties[43] and hyaline cartilage regeneration[44] using MSCs spheroids. Among various 3D culture techniques such as spinner flasks, rotating cell bioreactors, non-adherent plate, natural and synthetic matrices, chitosan films seem appealing for several reasons. This approach does not require expensive equipment and is cost-effective compared to non-adherent plates with synthetic matrices, since chitosan is a by-product of the

seafood industry. Culturing cells on chitosan films is technically easy. Combined, these advantages would allow clinical application on a large scale[45].

The bilateral patellar tendon model proposed here appears acceptable in terms of morbidity. No complication was observed in a recent study study. We were especially concerned over the risk of stressful effects induced by defects large enough to allow detectable biomechanical and histological changes. These concerns prompted the selection of rats over mice for this study based on previous studies related to the size and maturity of the tendon for preclinical injury models. A 'window defect' or central-third patellar tendon defect has been described in rabbits[46] and rats[30,31] to study tendon healing and augmentation. The patellar tendon 'window defect' model has been found reproducible for studying tendon repair in rats with histology[31,39], biomechanical testing[30,31], and *ex vivo* fluorescence imaging[31]. In this study, the size of the defect was equivalent to the central third of the patellar tendon, and was standardized with a 0.99 mm-diameter Kirschner wire as a template. These dimensions were adequate to study tendon healing without causing post-operative rupture. Because of their larger anatomic size versus mice, rats can accommodate larger defects, improving the reproducibility of injury, treatment delivery, and measures of outcome.

The analgesia protocol administered to the rats in this study was effective in controlling post-operative pain, as assessed with the RGS[37,38]. This scoring system was selected here because it was previously validated as detecting post-operative behavioral changes reflecting pain in rats[37,38]. The RGS is based on signs relatively simple to identify, such as orbital tightening, nose/cheek flattening, and ear/whisker changes. Rats also maintained a normal food intake throughout this study, which further supports the efficacy of this analgesia protocol. Indeed, previous reports have found a correlation between post-operative pain and body weight changes in rats treated with non-steroidal anti-inflammatories, such as meloxicam[47]. This agent was selected in this study and preemptive administration was derived from studies in rats[37,48] and dogs[49], where the administration of anti-inflammatory agents immediately prior to surgery has been found to attenuate surgically induced pain. Function was assessed as an additional indicator of post-operative pain, using a scoring system designed to evaluate the use of both pelvic limbs. The three activities selected here provide a general assessment of the range of motion and willingness to bear weight on the pelvic limbs. This scoring system was derived from both static and dynamic functional recovery studies in rats[50,51] and was designed to compare the time course of the functional outcomes observed. Scores indicate that the bilateral tendon defect induced a temporary decrease in function at 7 days, with a return to normal within 28 days. The function score appears more sensitive in detecting pain secondary to orthopedic conditions than the RGS. Similar functional tests have been used to evaluate tendon healing such as the Achilles Functional Index[28], paw and stride measures[51], or other macroscopic scoring systems[52].

This model was designed to reduce the number of animals enrolled in the study, while differentiating outcomes between untreated tendons and two stem cell-based treatments. The effects of the treatments tested in this study are discussed in another publication[36]. The model used here allowed detection of treatment differences through the use of an internal control in each rat, combined with non-destructive biomechanical testing of tendons at 28 days (data not presented here).

Activated conditioned plasma was selected because of its common use as a carrier for stem cells, biocompatibility, accessibility, and current clinical applications in the management of tendinopathies[53,54]. It may have contributed to the healing of treated tendons, but allowed local retention of stem cells, and it does not interfere with the comparison of treatment groups, since both included the same amount of activated conditioned plasma. The histological features of untreated tendons are consistent with previous descriptions of tendon healing, where necrotic tissue and disrupted collagen bundles are removed by phagocytosis and lytic enzymes by macrophages during the inflammation phase, which lasts up to 10 days post injury[54,55,56]. During the proliferative phase, cellular proliferation and vascularity of the repair site is greatest at 28 days after tendon repair[57,58]. We found a correlation between the apparent thickening of tendons, cross-sectional areas, and lower modulus of elasticity of specimens. Based on these results, the histological score seems to reflect tissue changes that may not be desirable and do not lead to biomechanical strength, such as disorganization of collagen fibers, angiogenesis, and chondrogenesis. In the future, the ability of this model to discriminate treatments based on histological characteristics may be improved by integrating additional criteria such as presence of tenocytes, extracellular matrix organization, proteoglycan content, and distribution of elastin fibers[52,59].

## Disclosures

The authors have no conflict of interest to disclose.

## Acknowledgements

The authors would like to acknowledge Dr. Su, PhD, for her statistical analysis of the data. The authors also thank Dr. McClure, DVM, PhD DACLAM, for her advice on the anesthesia and pain management protocols used in the study. This project was supported by grants from Western University of Health Sciences Office of the Vice President for Research (12678v) and USDA Section 1433 funds (2090).

## References

1. Rossdale, P. D., Hopes, R., Digby, N. J., & offord, K. Epidemiological study of wastage among racehorses 1982 and 1983. *Vet Rec.* **116** (3), 66-69 (1985).
2. Black, D. A., Tucci, M., Puckett, A., Lawyer, T., & Benghuzzi, H. Strength of a new method of achilles tendon repair in the rat - biomed 2011. *Biomed Sci Instrum.* **47** 112-117 (2011).
3. Lake, S. P., Ansorge, H. L., & Soslowsky, L. J. Animal models of tendinopathy. *Disabil Rehabil.* **30** (20-22), 1530-1541 (2008).
4. Frank, C. B. Ligament structure, physiology and function. *J Musculoskelet Neuronal Interact.* **4** (2), 199-201 (2004).
5. Godwin, E. E., Young, N. J., Dudhia, J., Beamish, I. C., & Smith, R. K. Implantation of bone marrow-derived mesenchymal stem cells demonstrates improved outcome in horses with overstrain injury of the superficial digital flexor tendon. *Equine Vet J.* **44** (1), 25-32 (2012).
6. Smith, R. K. *et al.* Beneficial effects of autologous bone marrow-derived mesenchymal stem cells in naturally occurring tendinopathy. *PLoS One.* **8** (9), e75697 (2013).

7. Fossett, E., Khan, W. S., Longo, U. G., & Smitham, P. J. Effect of age and gender on cell proliferation and cell surface characterization of synovial fat pad derived mesenchymal stem cells. *J Orthop Res.* **30** (7), 1013-1018 (2012).
8. Zaim, M., Karaman, S., Cetin, G., & Isik, S. Donor age and long-term culture affect differentiation and proliferation of human bone marrow mesenchymal stem cells. *Ann Hematol.* **91** (8), 1175-1186 (2012).
9. Leychkis, Y., Munzer, S. R., & Richardson, J. L. What is stemness? *Stud Hist Philos Biol Biomed Sci.* **40** (4), 312-320 (2009).
10. VandeVord, P. J. *et al.* Evaluation of the biocompatibility of a chitosan scaffold in mice. *J Biomed Mater Res.* **59** (3), 585-590 (2002).
11. Griffon, D. J., Abulencia, J. P., Ragetly, G. R., Fredericks, L. P., & Chaieb, S. A comparative study of seeding techniques and three-dimensional matrices for mesenchymal cell attachment. *J Tissue Eng Regen Med.* **5** (3), 169-179 (2011).
12. Schwartz, Z., Griffon, D. J., Fredericks, L. P., Lee, H. B., & Weng, H. Y. Hyaluronic acid and chondrogenesis of murine bone marrow mesenchymal stem cells in chitosan sponges. *Am J Vet Res.* **72** (1), 42-50 (2011).
13. Ragetly, G., Griffon, D. J., & Chung, Y. S. The effect of type II collagen coating of chitosan fibrous scaffolds on mesenchymal stem cell adhesion and chondrogenesis. *Acta Biomater.* **6** (10), 3988-3997 (2010).
14. Ragetly, G. R., Griffon, D. J., Lee, H. B., & Chung, Y. S. Effect of collagen II coating on mesenchymal stem cell adhesion on chitosan and on reacetylated chitosan fibrous scaffolds. *J Mater Sci Mater Med.* **21** (8), 2479-2490 (2010).
15. Ragetly, G. R. *et al.* Effect of chitosan scaffold microstructure on mesenchymal stem cell chondrogenesis. *Acta Biomater.* **6** (4), 1430-1436 (2010).
16. Ragetly, G. R., Slavik, G. J., Cunningham, B. T., Schaeffer, D. J., & Griffon, D. J. Cartilage tissue engineering on fibrous chitosan scaffolds produced by a replica molding technique. *J Biomed Mater Res A.* **93** (1), 46-55 (2010).
17. Slavik, G. J., Ragetly, G., Ganesh, N., Griffon, D. J., & Cunningham, B. T. A replica molding technique for producing fibrous chitosan scaffolds for cartilage engineering. *Journal of Materials Chemistry.* **17** (38), 4095-4101 (2007).
18. Griffon, D. J., Sedighi, M. R., Schaeffer, D. V., Eurell, J. A., & Johnson, A. L. Chitosan scaffolds: interconnective pore size and cartilage engineering. *Acta Biomater.* **2** (3), 313-320 (2006).
19. Huang, G. S., Dai, L. G., Yen, B. L., & Hsu, S. H. Spheroid formation of mesenchymal stem cells on chitosan and chitosan-hyaluronan membranes. *Biomaterials.* **32** (29), 6929-6945 (2011).
20. Cheng, N. C., Wang, S., & Young, T. H. The influence of spheroid formation of human adipose-derived stem cells on chitosan films on stemness and differentiation capabilities. *Biomaterials.* **33** (6), 1748-1758 (2012).
21. Webster, R. A., Blaber, S. P., Herbert, B. R., Wilkins, M. R., & Vesey, G. The role of mesenchymal stem cells in veterinary therapeutics - a review. *N Z Vet J.* **60** (5), 265-272 (2012).
22. Khan, M. H., Li, Z., & Wang, J. H. Repeated exposure of tendon to prostaglandin-E2 leads to localized tendon degeneration. *Clin J Sport Med.* **15** (1), 27-33 (2005).
23. Sullo, A., Maffulli, N., Capasso, G., & Testa, V. The effects of prolonged peritendinous administration of PGE1 to the rat Achilles tendon: a possible animal model of chronic Achilles tendinopathy. *J Orthop Sci.* **6** (4), 349-357 (2001).
24. van Schie, H. T. *et al.* Monitoring of the repair process of surgically created lesions in equine superficial digital flexor tendons by use of computerized ultrasonography. *Am J Vet Res.* **70** (1), 37-48 (2009).
25. Schramme, M., Kerekes, Z., Hunter, S., & Labens, R. Mr imaging features of surgically induced core lesions in the equine superficial digital flexor tendon. *Vet Radiol Ultrasound.* **51** (3), 280-287 (2010).
26. Hast, M. W., Zuskov, A., & Soslowsky, L. J. The role of animal models in tendon research. *Bone Joint Res.* **3** (6), 193-202 (2014).
27. Warden, S. J. Animal models for the study of tendinopathy. *Br J Sports Med.* **41** (4), 232-240 (2007).
28. Murrell, G. A. *et al.* Achilles tendon injuries: a comparison of surgical repair versus no repair in a rat model. *Foot Ankle.* **14** (7), 400-406 (1993).
29. Ozer, H. *et al.* [Effect of glucosamine chondroitine sulphate on repaired tenotomized rat Achilles tendons]. *Eklem Hastalik Cerrahisi.* **22** (2), 100-106 (2011).
30. Chan, B. P., Fu, S. C., Qin, L., Rolf, C., & Chan, K. M. Pyridinoline in relation to ultimate stress of the patellar tendon during healing: an animal study. *J Orthop Res.* **16** (5), 597-603 (1998).
31. Ni, M. *et al.* Tendon-derived stem cells (TDSCs) promote tendon repair in a rat patellar tendon window defect model. *J Orthop Res.* **30** (4), 613-619 (2012).
32. Orth, P., Zurakowski, D., Alini, M., Cucchiarini, M., & Madry, H. Reduction of sample size requirements by bilateral versus unilateral research designs in animal models for cartilage tissue engineering. *Tissue Eng Part C Methods.* **19** (11), 885-891 (2013).
33. Kajikawa, Y. *et al.* Platelet-rich plasma enhances the initial mobilization of circulation-derived cells for tendon healing. *J Cell Physiol.* **215** (3), 837-845 (2008).
34. Xu, W. *et al.* Human iPSC-derived neural crest stem cells promote tendon repair in a rat patellar tendon window defect model. *Tissue Eng Part A.* **19** (21-22), 2439-2451 (2013).
35. Taguchi, T. *et al.* Influence of hypoxia on the stemness of umbilical cord matrix-derived mesenchymal stem cells cultured on chitosan films. *J Biomed Mat Res B: Appl Biomat.* n/a-n/a (2017).
36. Griffon, D. J. *et al.* Effects of Hypoxia and Chitosan on Equine Umbilical Cord-Derived Mesenchymal Stem Cells. *Stem Cells Int.* **2016** 2987140 (2016).
37. Roughan, J. V., & Flecknell, P. A. Evaluation of a short duration behaviour-based post-operative pain scoring system in rats. *Eur J Pain.* **7** (5), 397-406 (2003).
38. Sotocinal, S. G. *et al.* The Rat Grimace Scale: a partially automated method for quantifying pain in the laboratory rat via facial expressions. *Mol Pain.* **7** 55 (2011).
39. Rosenbaum, A. J. *et al.* Histologic stages of healing correlate with restoration of tensile strength in a model of experimental tendon repair. *HSS J.* **6** (2), 164-170 (2010).
40. Vidal, M. A., Walker, N. J., Napoli, E., & Borjesson, D. L. Evaluation of senescence in mesenchymal stem cells isolated from equine bone marrow, adipose tissue, and umbilical cord tissue. *Stem cells and development.* **21** (2), 273-283 (2011).
41. Patterson-Kane, J., Becker, D., & Rich, T. The pathogenesis of tendon microdamage in athletes: the horse as a natural model for basic cellular research. *J Compar Pathol.* **147** (2), 227-247 (2012).
42. Dominici, M. *et al.* Minimal criteria for defining multipotent mesenchymal stromal cells. The. *Cytotherapy.* **8** (4), 315-317 (2006).
43. Bartosh, T. J. *et al.* Aggregation of human mesenchymal stromal cells (MSCs) into 3D spheroids enhances their antiinflammatory properties. *Proc Natl Acad Sci U S A.* **107** (31), 13724-13729 (2010).


 

44. Zhang, K., Yan, S., Li, G., Cui, L., & Yin, J. In-situ birth of MSCs multicellular spheroids in poly(L-glutamic acid)/chitosan scaffold for hyaline-like cartilage regeneration. *Biomaterials.* **71** 24-34 (2015).
45. Montanez-Sauri, S. I., Beebe, D. J., & Sung, K. E. Microscale screening systems for 3D cellular microenvironments: platforms, advances, and challenges. *Cellular and molecular life sciences : CMLS.* **72** (2), 237-249 (2015).
46. Butler, D. L. *et al.* The use of mesenchymal stem cells in collagen-based scaffolds for tissue-engineered repair of tendons. *Nat Protoc.* **5** (5), 849-863 (2010).
47. Brennan, M. P., Sinusas, A. J., Horvath, T. L., Collins, J. G., & Harding, M. J. Correlation between body weight changes and postoperative pain in rats treated with meloxicam or buprenorphine. *Lab Anim (NY).* **38** (3), 87-93 (2009).
48. Ramon-Cueto, A., Cordero, M. I., Santos-Benito, F. F., & Avila, J. Functional recovery of paraplegic rats and motor axon regeneration in their spinal cords by olfactory ensheathing glia. *Neuron.* **25** (2), 425-435 (2000).
49. Arculus, S. L. Use of meloxicam as an analgesic in canine orthopaedic surgery. *Vet Rec.* **155** (24), 784 (2004).
50. Bervar, M. Video analysis of standing--an alternative footprint analysis to assess functional loss following injury to the rat sciatic nerve. *J Neurosci Methods.* **102** (2), 109-116 (2000).
51. Perry, S. M., Getz, C. L., & Soslowsky, L. J. Alterations in function after rotator cuff tears in an animal model. *J Shoulder Elbow Surg.* **18** (2), 296-304 (2009).
52. Stoll, C. *et al.* Healing parameters in a rabbit partial tendon defect following tenocyte/biomaterial implantation. *Biomaterials.* **32** (21), 4806-4815 (2011).
53. Hankemeier, S. *et al.* Bone marrow stromal cells in a liquid fibrin matrix improve the healing process of patellar tendon window defects. *Tissue Eng Part A.* **15** (5), 1019-1030 (2009).
54. Silver, I. A. *et al.* A clinical and experimental study of tendon injury, healing and treatment in the horse. *Equine Vet J Suppl.* (1), 1-43 (1983).
55. Enwemeka, C. S. Inflammation, cellularity, and fibrillogenesis in regenerating tendon: implications for tendon rehabilitation. *Phys Ther.* **69** (10), 816-825 (1989).
56. Goldin, B., Block, W. D., & Pearson, J. R. Wound healing of tendon--I. Physical, mechanical and metabolic changes. *J Biomech.* **13** (3), 241-256 (1980).
57. Lyras, D. N. *et al.* The effect of platelet-rich plasma gel in the early phase of patellar tendon healing. *Arch Orthop Trauma Surg.* **129** (11), 1577-1582 (2009).
58. Oshiro, W., Lou, J., Xing, X., Tu, Y., & Manske, P. R. Flexor tendon healing in the rat: a histologic and gene expression study. *J Hand Surg Am.* **28** (5), 814-823 (2003).
59. Visser, L. C., Arnoczky, S. P., Caballero, O., & Gardner, K. L. Evaluation of the use of an autologous platelet-rich fibrin membrane to enhance tendon healing in dogs. *Am J Vet Res.* **72** (5), 699-705 (2011).


 